

# Supplementary Information to *A Simple Landscape of Metastable State Energies for Two-Dimensional Cellular Matter*

Sangwoo Kim and Sascha Hilgenfeldt

## 1 Simulation Protocols

### 1.1 Preparation of Initial Configurations

A set of  $N$  seed points in a rectangular periodic box is generated and the corresponding Voronoi diagrams are used as initial configurations for SE simulations. Three different point processes are adopted to generate a rich variety of topological structures: Perturbed lattice algorithm, Lloyd's algorithm, and Excluded-volume algorithm. The perturbed lattice algorithm displaces regular triangular lattice points randomly by Gaussian noise with a standard deviation  $\alpha$ . As  $\alpha$  increases, the perturbed point pattern becomes more disordered and the corresponding Voronoi diagram contains a larger number of defects, i.e.,  $\mu_{20}$  increases. The Lloyd's algorithm regularizes random Poisson point patterns through a prescribed number  $n_L$  of Lloyd iterations. Each iteration updates the point pattern by taking the centroid positions of Voronoi cells. A larger  $n_L$  generates a more ordered Voronoi tessellation and smaller  $\mu_{20}$ . The excluded-volume algorithm places  $N$  disks with radius  $r$  consecutively in the periodic box and a new disk position is accepted only if there is no overlap with previously generated disks. The point patterns and Voronoi diagrams become more regular as  $r$  increases, reducing  $\mu_{20}$ . Varying  $\alpha$ ,  $n_L$ , and  $r$  in these point processes, we can prepare initial configurations with a wide range of  $\mu_{20}$ . None of the results are sensitive to the particular preparation protocol.

### 1.2 Target Area Assignment

Target area values are randomly generated from a gamma distribution with a given area polydispersity  $c_A$  (using other distribution shapes, such as log-normal, does not change the presented outcomes). When the target area values are assigned randomly to initial Voronoi cells, there is no correlation between size and topology, i.e., the resulting covariance  $\mu_{11}$  is close to 0. On the other hand, the maximum covariance  $\mu_{11}^{max}$  can be approached by assigning area values strictly in order of initial Voronoi cell topologies. If a fraction of initial Voronoi cells  $n_c = N_c/N$  is chosen and their area values are assigned in the order of topology while the remaining cell areas are assigned randomly, the covariance lies between 0 and  $\mu_{11}^{max}$ . Hence, any positive

$\mu_{11}$  between 0 and  $\mu_{11}^{max}$  can be imposed on the initial configuration by changing  $n_c$ . Likewise, any negative  $\mu_{11} > -\mu_{11}^{max}$  can be attained by assigning  $N_c$  area values in the reverse order of topology, although most  $\mu_{11} < 0$  structures prove to be unstable states. There is no systematic difference in MS energies between area assignment strategies.

### 1.3 Eliminating unstable states and Annealing

Discrepancies between the initial Voronoi cell area and the target area induce a large degree of area adjustment in initial energy minimization steps of SE simulations and thus generate a plethora of unstable four-way vertices. These configurations are unstable (not metastable states), and the four-way vertices are relaxed to two regular three-way vertices by T1 transitions. In our simulations, we define a critical length  $L_c$ , so that any edges shorter than  $L_c$  undergo this four-way vertex treatment. Typically, we choose  $L_c = 0.01\mathcal{L}_0$ , but results are insensitive to the particular choice. In addition to generating initial metastable states, further MS can be generated by inducing T1 transitions of edges longer than  $L_c$ . In particular, we commonly use the greedy algorithm that performs a T1 transition on the currently shortest edge in the sample. This algorithm is an efficient method for annealing metastable states to the ground state because there is a positive correlation between local edge length and energy difference between two adjacent metastable states [1]. With various initial configurations, different area assignments, and the annealing algorithm, we cover the entire configuration space of metastable states in multiple ways and find the robust correlations between metastable states energy and statistical measures described in the main text.

## 2 Relating Governing Energy Functionals to Equivalent Foam Energy

The equivalent foam energy  $\epsilon_f^*$  is used as a quantitative measure of metastable state energy that can be compared across very different systems. In this section, we show that  $\epsilon_f^*$  is strongly correlated with the actual mechanical energy that determines metastable states, so that a particular  $\epsilon_f^*$  implies a particular mechanical energy value. In the tissue model, the governing energy functional  $\epsilon_t$  differs significantly from  $\epsilon_f^*$  and, unlike the foam energy, contains the parameter  $\gamma$ , see Eq. (2) of the main text. Rewriting  $\epsilon_t$ , we get

$$\epsilon_t = \frac{1}{6N\mathcal{L}_0} \left( \sum_i \frac{(P_i - P_{i,0})^2}{P_{i,0}} - \gamma \sum_i P_i \right) = \frac{1}{6N\mathcal{L}_0} \left( \sum_i \frac{P_i^2}{P_{i,0}} - \sum_i (\gamma + 2)P_i + \sum_i P_{i,0} \right). \quad (1)$$

The linear term is proportional to the equivalent foam energy. Assuming that the ratio of  $P_i$  to  $P_{i,0}$  stays approximately constant for all domains, the sum of squared perimeters  $\sum_i P_i^2$  can be approximated as a square of the perimeter sum, which yields

$$\epsilon_t \approx \frac{1}{6N\mathcal{L}_0} \left( \frac{(\sum_i P_i)^2}{\sum_i P_{i,0}} - \sum_i (\gamma + 2)P_i + \sum_i P_{i,0} \right) = \frac{(\epsilon_f^*)^2}{\epsilon_c} - (\gamma + 2)\epsilon_f^* + \epsilon_c, \quad (2)$$

where we have defined  $\epsilon_c \equiv \frac{1}{6N\mathcal{L}_0} \sum_i P_{i,0}$ . The equilibrium perimeter  $P_{i,0}$  is the equivalent circle perimeter for a given area,  $P_{i,0} = 2\sqrt{\pi A_i}$ . By definition, the perimeter length  $6\mathcal{L}_0$  of a regular hexagon of the average

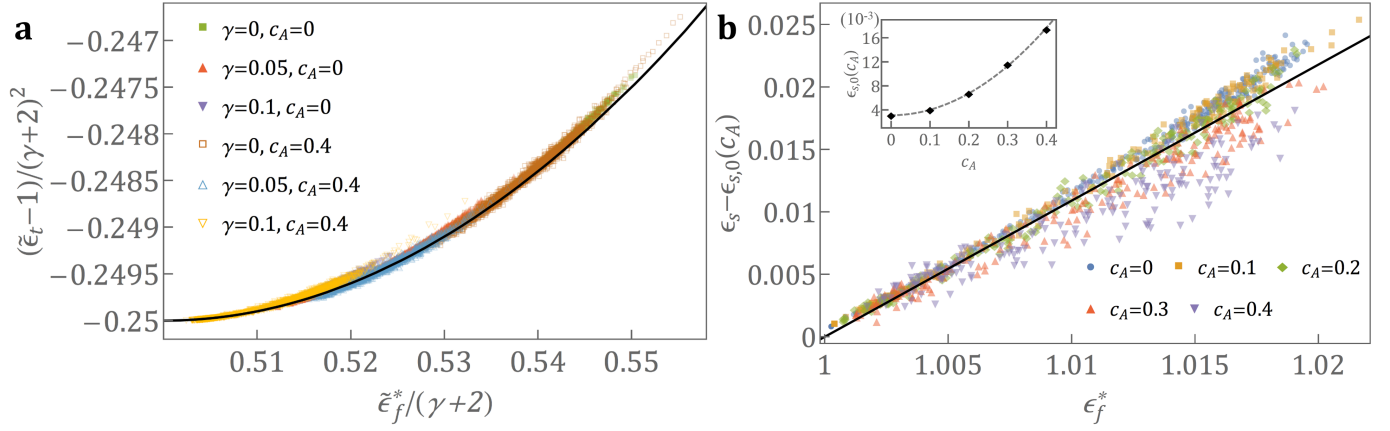


**Figure S1:** The equivalent foam energy accurately predicts (a) tissue energy and (b) spring energy. The inset in (b) shows the  $c_A$  dependence of  $\epsilon_{s,0}$ .

area  $\bar{A} = 1$  is equal to  $2\sqrt{2\sqrt{3}}$ . Hence,  $\epsilon_c$  is proportional to the expectation value of the square root of areas  $\sqrt{A} = \sum_i \sqrt{A_i}/N$ ,

$$\epsilon_c = \sqrt{\frac{\pi}{2\sqrt{3}} \frac{\sum_i \sqrt{A_i}}{N}} \quad (3)$$

If the area distribution is taken to be a gamma distribution with a given polydispersity  $c_A$ , as in most of our simulations,  $\epsilon_c$  can be estimated analytically as

$$\epsilon_c = \sqrt{\frac{\pi}{2\sqrt{3}} \frac{\sum_i \sqrt{A_i}}{N}} \approx \sqrt{\frac{\pi}{2\sqrt{3}} \int_0^\infty \sqrt{A} P(A) dA} = \sqrt{\frac{\pi}{2\sqrt{3}} \frac{c_A \Gamma(c_A^{-2} + \frac{1}{2})}{\Gamma(c_A^{-2})}} \quad (4)$$

Further normalizing  $\tilde{\epsilon}_f^* \equiv \epsilon_f^*/\epsilon_c$ ,  $\tilde{\epsilon}_t \equiv \epsilon_t/\epsilon_c$ , the above relation is

$$\frac{\tilde{\epsilon}_t - 1}{(\gamma + 2)^2} = \left( \frac{\tilde{\epsilon}_f^*}{\gamma + 2} \right)^2 - \frac{\tilde{\epsilon}_f^*}{\gamma + 2}, \quad (5)$$

which proves an excellent approximation to the simulation data for all  $\gamma < \gamma_c$  (Fig. S1a). Hence, the energy landscape of  $\epsilon_f^*$  can be translated to that of  $\epsilon_t$  analytically. While the spring energy  $\epsilon_s$  cannot be easily analytically translated to  $\epsilon_f^*$ , we find an empirical linear correlation between  $\epsilon_s$  and  $\epsilon_f^*$  up to  $c_A \lesssim 0.4$ ,

$$\epsilon_s - \epsilon_{s,0}(c_A) \approx 1.09(\epsilon_f^* - 1) \quad (6)$$

$$\epsilon_{s,0}(c_A) \approx 0.091c_A^2 - 0.00312 \quad (7)$$

Therefore,  $\epsilon_f^*$  can also be used as a predictor for energy in the spring system, as illustrated in Fig. S1b.

### 3 Estimation of $M_{20}$ from Local Defect Configurations

Two local defect structures in a monodisperse foam are considered in order to estimate  $M_{20}$ . The quadruple defect configuration (two adjacent dislocations, Fig. S2a) is obtained by executing one T1 transition

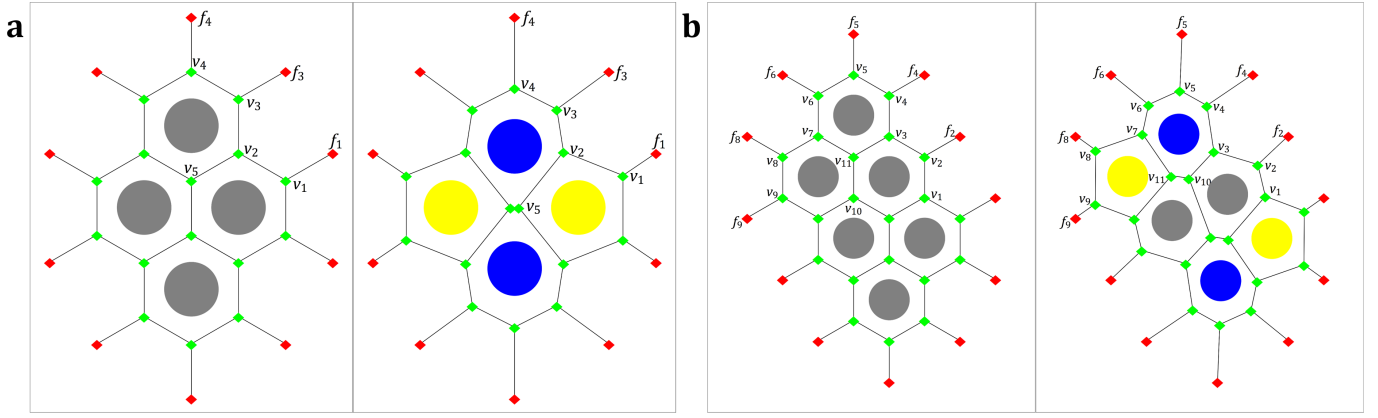


**Figure S2:** Schematics of local defect configurations. (a) Quadruple defect and corresponding hexagonal configuration; (b) Two separated dislocations with the corresponding hexagonal configuration.

starting from the regular honeycomb. A second T1 transition then separates the quadruple defect into two dislocations separated by a layer of hexagonal domains (Fig. S2b). Assuming in both cases that these defect configurations remain embedded in the background of a regular honeycomb, they both have  $\mu_{20} = \frac{4}{N}$ . As the effect of T1 transitions decays exponentially with distance from the T1 edge [1], the energies of these configurations can be approximated from local edge length changes.

Assuming that vertices of the cells involved in the defect configuration (green in Fig. S2) are free to adjust for minimizing the domain energy, while background vertices (red in Fig. S2) are fixed at the position of the regular honeycomb, the local energy minimum structure can be analytically computed.

In the case of the quadruple defect, there are five vertices that are free to adjust their positions ( $x_i, y_i$ ) to minimize system energy but symmetries about the  $x$ - and  $y$ -axes reduce the degrees of freedom to eight. The target areas  $A_0 = 1$  of the cells are enforced by two Lagrange multipliers  $\lambda_5$  and  $\lambda_7$ . The foam energy of the quadruple defect configuration is then written explicitly as

$$\epsilon_f^{(1)} = 1 + \frac{1}{3N\mathcal{L}_0} (4L_{12} + 4L_{23} + 4L_{34} + 4L_{25} + 4y_1 + 2x_5 + 4L_1 + 4L_3 + 2L_4 - 29\mathcal{L}_0) + \lambda_5(A_5 - A_0) + \lambda_7(A_7 - A_0), \quad (8)$$

$L_{ij}$  and  $L_k$  are edge lengths between vertices  $v_i$  and  $v_j$ , and between vertex  $v_k$  and the fixed vertex  $f_k$ , respectively (cf. Fig. S2).  $A_5$  and  $A_7$  are the areas of the pentagon and heptagon, which can be computed analytically by their vertex coordinates,

$$A_{5,7} = \frac{1}{2} \sum_i \begin{vmatrix} x_i & x_{i+1} \\ y_i & y_{i+1} \end{vmatrix}$$

An equilibrium state (extremum of  $\epsilon_f^{(1)}$ ) is obtained by solving the system of 10 equations  $\frac{\partial \epsilon_f^{(1)}}{\partial x_i} = 0$ ,  $\frac{\partial \epsilon_f^{(1)}}{\partial y_j} = 0$ , and  $\frac{\partial \epsilon_f^{(1)}}{\partial \lambda_k} = 0$ . Employing Newton's method in Mathematica, we find vertex coordinates and the minimum energy. The quadruple defect induces an energy increase  $\Delta \epsilon_f^{(1)} = \epsilon_f^{(1)} - \epsilon_0$  over the regular honeycomb energy, while the topological variance increases by  $\Delta \mu_{20} = \frac{4}{N}$ . Under the assumption of linearity between  $\epsilon_f$  and  $\mu_{20}$ , we obtain  $\Delta \epsilon_f^{(1)} / \Delta \mu_{20} = M_{20}^{(1)} = 0.031$ .

The local energy minimum configuration of the two dislocations configuration is computed in the same way. There are eleven free vertices and the domain areas are fixed by three Lagrange multipliers. The local minimum energy  $\epsilon_f^{(2)}$  follows from solving a system of 25 equations, yielding  $M_{20}^{(2)} = 0.045$ . More complicated configurations could also be computed analytically, but these common prototypes show that the energy changes are likely to be in the same range. The empirical result  $M_{20} = 0.041$  from a large number of simulations is bracketed by the two prototypical values.

## 4 Analytic Computation of Maximum Covariance $\mu_{11}^{max}$

Practically, configurations of maximum covariance  $\mu_{11}^{max}$  are obtained by assigning target area values in the order of number of neighbors when preparing a MS in simulations. To make analytical progress, we adopt a normal (Gaussian) approximation of the area probability distribution  $P(A)$ , which in the granocentric model [2] yields explicit predictions for the neighbor probability  $P(n)$ ,

$$P(n) = \psi_{n+1}(x) - \psi_n(x) \quad (9)$$

$$\psi_{n+1}(x) = \frac{1}{2} \operatorname{erf} \left[ \frac{\beta}{x} (2n - 1) \right]. \quad (10)$$

In the granocentric model, valid at the ground state,  $x = c_A$  corresponds to  $c_A$ . Here, we take  $x$  as a control parameter to change  $\mu_{20}$  at given  $c_A$  for metastable-state calculations. For improved accuracy, we use a best fit for the constant  $\beta$  from the ground state  $\mu_{20}(c_A)$  data (Fig. S3), which yields  $\beta \approx 0.206$ , slightly larger than the parameter-free  $\beta_0 = \sqrt{2\pi^2/585}$  [2]. We constrain the range of  $n$  to the practical  $n \in \{2, \dots, 10\}$ , and the range of  $x$  in our calculation is between 0 and 0.9 to ensure  $\sum_n P(n) = 1$  and  $\bar{n} = 6$ .  $P(n)$  is symmetric around  $n = 6$ , so  $P(6 - n) = P(6 + n)$ , while  $\psi_2(x) \approx -\frac{1}{2}$  and  $\psi_{11}(x) \approx \frac{1}{2}$  to excellent accuracy. The variance of the neighbor distribution  $\mu_{20}$  can then be written as

$$\mu_{20} = \sum_{n=2}^{10} (n - 6)^2 P(n) = 2 \left( 8 + 7\psi_3(x) + 5\psi_4(x) + 3\psi_5(x) + \psi_6(x) \right) \quad (11)$$

or explicitly

$$\mu_{20} = \sum_{n=1}^4 (2n - 1) \operatorname{erfc} \left[ \frac{\beta}{x} (2n - 1) \right] \quad (12)$$

The probability density and cumulative distribution functions for the normal area distribution are

$$P(A) = \frac{1}{c_A \sqrt{2\pi}} \exp \left[ -\frac{(A - 1)^2}{2c_A^2} \right], \quad (13)$$

$$F(A) = \frac{1}{2} \left( 1 + \operatorname{erf} \left[ \frac{A - 1}{\sqrt{2}c_A} \right] \right), \quad (14)$$

respectively. When target area values are assigned in the order of topology for maximum covariance, the range of area for domains with  $n$  neighbors,  $A_{n-1} < A < A_n$ , can be analytically computed. The range of  $n$

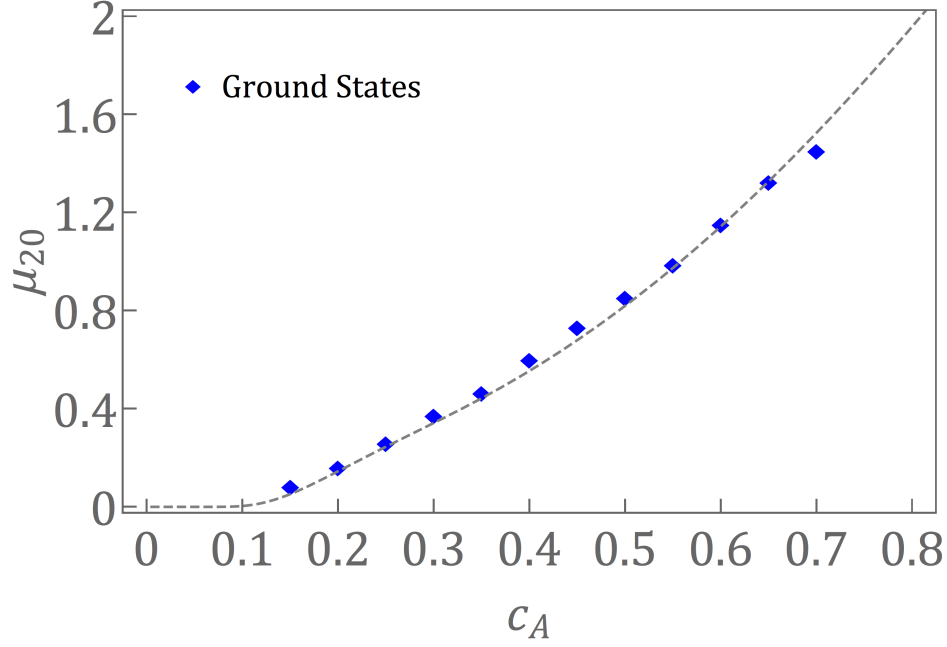


**Figure S3:** Size-topology correlation. The expression (12) with  $x = c_A$  (dashed line) is an excellent approximation to simulation data from the lowest-energy states (symbols), with the constant  $\beta$  obtained from a least-square fit.

fixes  $A_1 = -\infty$  and  $A_{10} = \infty$ . The cumulative probability of  $A < A_k$  must equal the cumulative probability  $\sum_{n < k} P(n)$ , so that

$$F(A_k) = \sum_{n < k} P(n) = \frac{1}{2} + \psi_{k+1}(x) \quad (15)$$

The matching functional forms of  $F(A)$  and  $\psi_k$  yield the equality

$$A_k = 1 + \frac{\sqrt{2}c_A\beta}{x}(2k - 11). \quad (16)$$

To compute  $\mu_{11}$ , we make use of

$$\mu_{11} = \overline{(n-6)(A-1)} = \overline{nA} - 6, \quad (17)$$

$$\overline{nA} = \sum_{n=2}^{10} n \int_{A_{n-1}}^{A_n} AP(A) dA. \quad (18)$$

The latter can be rewritten as

$$\overline{nA} = \sum_{n=2}^{10} n(G(A_n) - G(A_{n-1})) = 10 - \sum_{n=2}^9 G(A_n), \quad (19)$$

with a function  $G(A_n)$  defined as

$$G(A_n) = \int_{-\infty}^{A_n} AP(A) dA = \frac{1}{2} \left( 1 + \operatorname{erf} \left[ \frac{A_n - 1}{\sqrt{2}c_A} \right] \right) - \frac{c_A}{\sqrt{2\pi}} \exp \left[ -\frac{(A_n - 1)^2}{2c_A^2} \right]. \quad (20)$$

From (16), (17), (19), and (20), one obtains

$$\mu_{11}^{max} = c_A \sum_{n=1}^4 \sqrt{\frac{2}{\pi}} \exp \left[ -\frac{\beta^2}{x^2} (2n - 1)^2 \right], \quad (21)$$

which, together with (12), yields the desired parametric expression for the maximum covariance.

## 5 Hexagonal polydisperse configurations

The hexagonal configuration serves as a special point in the energy landscape because the energy is invariant against changes in area polydispersity. This can be understood from area adjustment of an individual hexagon. The hexagon area can be increased (or decreased) by parallel movement of all edges; all such configurations are still local mechanical equilibria because the  $120^\circ$  angles between edges are conserved. If the hexagon area is dilated, the edges of an hexagon are lengthened by  $2\Delta L_2$  while the branching edges are shortened by  $\Delta L_1$  (see Fig. S4a). However, as the angle between adjoining edges is always  $2\pi/3$ ,  $\Delta L_1 = 2\Delta L_2$ , and the total edge length change is zero. This illustrates that any area adjustment of an individual hexagon does not induce a foam energy change. Any polydisperse hexagonal configuration can be attained by superposing individual hexagon area adjustments and these steps are all energy-neutral. Hence, the hexagonal configuration energy stays at  $\epsilon_0 = 1$  independent of  $c_A$ . When the areas of the polydisperse hexagons be-

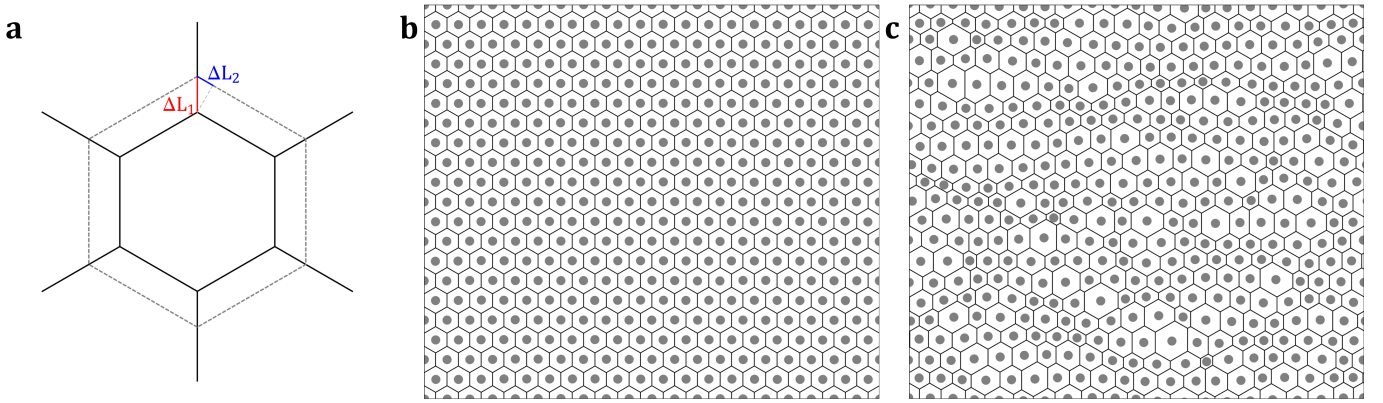


**Figure S4:** Polydisperse hexagonal foam. (a) Schematics of the area dilation for a hexagon. The edge length increase of the hexagon is compensated by shortening of branching edges. Equilibrium hexagonal configurations are shown for  $c_A = 0$  (b) and  $c_A = 0.3$  (c). SE simulations confirm that the domain energy of hexagonal configurations stays at  $\epsilon_0$  for different area polydispersity.

come too disparate, four-way junctions (and thus a topological transition) will be generated, and the statement of constant energy ceases to be true. Empirically, this happens when  $c_A \geq 0.45$ , and this is where the linear theoretical energy functional  $\epsilon_f^{th}$  should cease to be universal. In practice, some predictions remain quantitatively valid for significantly larger  $c_A$ , cf. the values of minimum and maximum energy in Fig. 3c of the main text.

## 6 Derivation of Critical Equivalent Foam Energy for a Given $\gamma$

A tissue system with a given  $\gamma$  acquires degenerate ground states when each domain perimeter can approach the value of  $(1 + \frac{\gamma}{2})P_{i,0}$ . The corresponding critical equivalent foam energy is the sum of these perimeters over all cells,

$$\epsilon_{f,c}^* = \frac{1}{6N\mathcal{L}_0} \sum_i \left(1 + \frac{\gamma}{2}\right) P_{i,0}. \quad (22)$$

The sum over the equilibrium perimeters was approximated as  $\epsilon_c$  in Eq. (4) of the Supplementary Information. Thus we obtain

$$\epsilon_{f,c}^*(c_A) \approx \left(1 + \frac{\gamma}{2}\right) \sqrt{\frac{\pi}{2\sqrt{3}}} \frac{c_A \Gamma(c_A^{-2} + \frac{1}{2})}{\Gamma(c_A^{-2})} \quad (23)$$

When this energy value reaches the maximum possible energy for metastable states, all configurations become floppy ground states. This condition  $\epsilon_f^{*max}(c_A) = \epsilon_{f,c}^*(c_A)$  can be solved for the critical  $\gamma = \gamma_u$  for this unconditional loss of rigidity. In the range of  $c_A \in [0, 0.45]$ ,  $\gamma_u$  increases very weakly from  $\gamma_u = 0.195$  for  $c_A = 0$  to  $\gamma_u = 0.205$  for  $c_A = 0.45$ .

## References

- [1] Sangwoo Kim, Yiliang Wang, and Sascha Hilgenfeldt. Universal features of metastable state energies in cellular matter. *Physical Review Letters*, 120(24):248001, 2018.
- [2] Matthew P. Miklius and Sascha Hilgenfeldt. Analytical results for size-topology correlations in 2d disk and cellular packings. *Phys. Rev. Lett.*, 108:015502, Jan 2012.